Effects of Overload and Underload on the Residual Stress, Crack Plasticity, and the Crack Growth Rate

S.Y. Lee [1], H. Choo [1], P.K. Liaw [1], R.B. Rogge [2], and M.A. Gharghouri [2]

[1] Department of Materials Science and Engineering, The University of Tennessee, Knoxville, TN USA 37996

[2] Canadian Neutron Beam Centre, National Research Council, Chalk River Laboratories, Chalk River, ON, Canada K0J 1J0

Introduction

Many structural materials are subjected to variable-amplitude fatigue loading rather than constant-amplitude fatigue loading. Sudden changes in the cyclic loading patterns during fatigue deformation could give rise to complicated plastic zones in the vicinity of the crack tip and result in a considerable acceleration or retardation in the crack growth rate owing to these load interaction effects. Therefore, a fundamental understanding of the overload or underload effects and damage mechanisms will help enhance the lifetime prediction capabilities and improve the damage tolerance design for critical application exposed to random fatigue loadings. As a simple example, when a single tensile overload is applied during cycling loading, the crack growth rate slows down, which increases fatigue lifetime tremendously. Although much attention has been devoted to explain the retardation mechanism since its discovery in 1961, the phenomenon is still not fully understood. Due to the lack of experimental capabilities to measure the strain and stress fields within the bulk as a function of the distance from crack tip, the relationship between the overload or underload and the retardation or acceleration has not been quantitatively established.

Methods

In order to study the effects of overloading, underloading, and their combination on the constant-amplitude fatigue-crack growth [i.e., P_{max}: 8,880 N, P_{min}: 89 N, a load ratio, R: 0.01, where $R = P_{min} / P_{max}$)], a single tensile overload (i.e., $P_{overload}$: 13,320 N, which is 150% of P_{max}), a single compressive underload (i.e., $P_{underload}$: -13,320 N) and a set of mixed loads (i.e., overload-underload and underload-overload) were imposed systematically when the crack length reached 16 mm. After applying various loading conditions, a constant-amplitude fatigue experiment was resumed.

The crack growth rate (*da/dN*) versus stress-intensity factor range (ΔK) for the five different loading cases is shown in Figure 1. During a constant-amplitude fatigue-crack growth (*Case 1*), the crack growth rate increases linearly with increasing ΔK. After a single tensile overload (*Case 2*), there was an instantaneous acceleration of the crack growth rate followed by a large retardation period, resulting in a temporary decrease in the crack growth rates. On the other hand, after a single compressive underload (*Case 3*), a brief acceleration of the crack growth rate was observed. However, subsequent crack growth rates were very comparable to those of *Case 1*. When a compressive underload was imposed immediately after a tensile overload, a retardation period was still found but had a significantly reduced extent (*Case 4*). Finally, when a tensile overload was imposed immediately after a compressive underload (*Case 5*), the crack-growth rates were similar to those of a single tensile overload (*Case 2*), indicating a large retardation period.

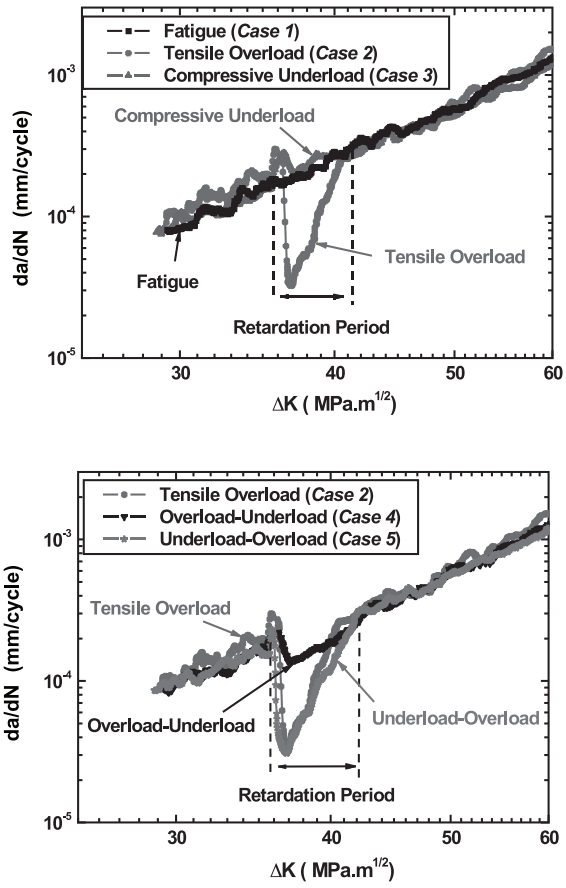

Fig. 1 The changes in the crack growth rate (*da/dN*) as a function of stress-intensity-factor range (ΔK) for the five different loading cases.

A neutron diffraction measurement was performed to probe the retardation or acceleration mechanism during fatigue crack growth following overload or underload using L3 spectrometer. High penetration capabilities and volume averaging of neutron diffraction technique allow mapping of the bulk residual strain and stress as a function of the distance from the crack tip. The five compact-tension (CT) specimens under different loading conditions [i.e., constant-amplitude fatigue (*Case 1*), tensile overloading (*Case 2*), compressive underloading (*Case 3*),

tensile overloading-compressive underloading (*Case 4*), and compressive underloading-tensile overloading (*Case 5*)] were prepared to study the influences of residual stresses on the crack growth rate (Figure 2).

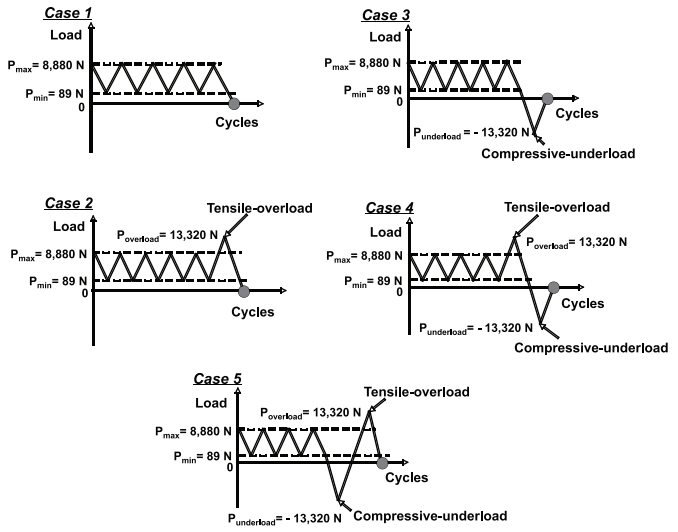

Fig. 2 *Neutron strain mapping was performed at the marked point right after five different loadings were applied.*

The spatially-resolved neutron strain scanning was performed to measure three principal residual-strain components. A total of 26 points were measured as a function of the distance from the crack tip (Figure 3). To provide the required spatial resolution, we used scanning intervals of 1 mm from -4 to 0 mm (crack tip), 0.5 mm from 0 to 8 mm where sharp strain gradients are expected, 2 mm from 8 to 16 mm, and 3 mm from 16 to 22 mm. The wavelength in each direction was selected from the Ge115 monochromator.

For X-longitudinal and the Y-transverse strain components, the wavelength of 1.3 Å was selected, and the specimens were aligned 53° (clockwise) from the incident neutron beam and the (311) diffraction pattern was recorded in a stationary detector with diffraction angles 2θ = 74°.

Thus for the X-longitudinal strain component, the diffraction vectors were parallel to longitudinal direction, parallel to the crack growth direction (X), of the specimen. The incident beam was defined by 1 mm wide and 2 mm tall (parallel to Y) slits, and the diffracted beams were collimated by 1 mm wide slit.

For Y-transverse strain component, the diffraction vectors were parallel to transverse direction (parallel to Y) of the specimen. The incident beam was defined by 2 mm wide and 1 mm tall (parallel to X) slits, and the diffracted beams were collimated by 2 mm wide slit.

For Z-normal strain component, the wavelength of 1.74 Å was selected. The specimens were aligned 127° (clockwise) from the incident neutron beam and the (311) diffraction pattern was recorded in a stationary detector with diffraction angles 2θ = 106°. Therefore, the diffraction vectors were parallel to normal direction (parallel to Z) of the specimen. The incident beam was defined by 2 mm wide and 1 mm tall (parallel to X) slits, and the diffracted beams were collimated by 2 mm wide slit.

The interplanar spacing (*d*-spacing) was determined from the Gaussian fitting of the (311) diffraction peak and the lattice strain was obtained from

$$\varepsilon = (d-d_0)/d_0 \quad (1)$$

where d_0 is the stress-free reference *d*-spacing, which was measured away from the crack-tip at a corner of each CT specimen. Three residual stress components, σ_i ($i = x, y, z$, corresponding to longitudinal, transverse and normal directions, respectively), are calculated from three strain components using the following equation:

$$\sigma_i = \frac{E}{1+\nu}\left[\varepsilon_i + \frac{\nu}{1-2\nu}\left(\varepsilon_x + \varepsilon_y + \varepsilon_z\right)\right] \quad (2)$$

where E is the Young's modulus and ν is the Poisson's ratio.

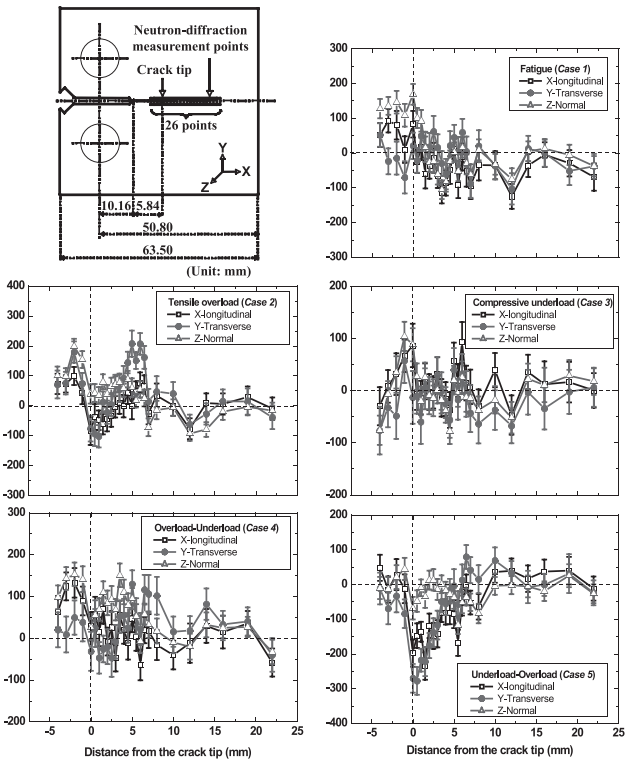

Fig. 3 *Geometry of a compact-tension specimen of Hastelloy C-2000 alloy and residual stress distributions in the vicinity of the crack tip for the five different loading cases.*

Figure 3 shows the residual stress profiles around a crack tip after five different loadings (indicated in Figure 2). Note that Y-transverse stress is the most sensitive stress for crack closure study and is reported here. In the case of constant-amplitude fatigue (*Case 1*), the compressive residual stress of -70 MPa was examined at the 1 mm behind of the crack tip and no compressive stress was found at the region ahead of the crack tip.

After a single tensile overload was applied (*Case 2*), compressive residual stresses with the maximum of -102 MPa were measured within about 1.5 mm in front of the crack tip, which will reduce the crack-tip driving force, and, thus, will retard the crack propagation.

After a single compressive underload was introduced (*Case 3*), the tensile residual stress of 60 MPa was examined at 1 mm behind of the crack tip. The residual stress distributions at *Case 3* were very similar to those at *Case 1* but showed tensile stress at 1 mm behind the crack tip. It is expected that this tensile stress will result in the decrease of the crack opening level, and, hence, higher crack-tip driving force for crack growth. Therefore, immediately after a single compressive underload, an instantaneous acceleration of crack growth would be observed.

When a compressive underload was imposed right after a tensile overload (*Case 4*), relatively small compressive residual stresses (with the maximum of -47 MPa) were examined within 3 mm in front of the crack tip. It is believed that such reduced compressive residual stresses resulted in the reduced retardation period, as compared to the single tensile overloading case (*Case 2*).

When a tensile overload was applied immediately after a compressive underload (*Case 5*), large compressive residual stresses were found within ± 6 mm near a crack tip. At 0.5 mm in front of the crack tip, the largest compressive stress of -280 MPa was examined, which will significantly retard the crack propagation. It can be noted that different crack growth behaviors are closely correlated with the distinct residual stress distributions around a crack tip under the various loading conditions.

Conclusion

From spatially-resolved strain scanning measurements, bulk residual stresses were successfully measured as a function of the distance from the crack tip, which allowed us to determine the kind and magnitude of residual stresses around a crack tip. The results will help us establish the relationship between crack-tip driving force and crack growth rate.